Upper-Hybrid Resonance Absorption, Emission, and Heating of an Afterglow Plasma Column

R. L. Stenzel* and R. W. Gould†
California Institute of Technology, Pasadena, California 90024
(Received 22 March 1971)

Microwave absorption and emission and electron temperatures of a nonuniform axially magnetized afterglow plasma column in a waveguide geometry have been investigated experimentally. Frequency ω and magnetic field ω_c are chosen to satisfy the upper-hybrid resonance condition $\omega^2=\omega_c^2+\omega_p^2(r)$, where $\omega_p(r)$ is the local electron plasma frequency. Nearly perfect absorption is observed in the range of upper-hybrid frequencies, while at other frequencies the absorption coefficient is essentially zero. The sharp absorption onset at the maximum upper-hybrid frequency yields an accurate measure for the peak electron density. Density decay and profile in the plasma column are observed—the latter using a new technique. In the range of high absorption the noise emission approaches the blackbody limit. The electron temperature is measured with a radiometer and a reference noise source in a new technique yielding both spatial and time dependence without perturbing the plasma. The time resolution is obtained by a sampling technique. The spatial resolution results from the fact that upper-hybrid resonance absorption and emission are confined to a narrow resonant layer. This property is also used to heat the electrons locally and observe the thermalization process.

I. INTRODUCTION

An experimental investigation of the interaction of guided microwaves with a low-temperature, inhomogeneous, magnetized plasma column is presented. Electron density and magnetic field are chosen such that the upper-hybrid resonance occurs at the signal frequency $\omega^2=\omega_c^2+\omega_p^2$. Column radius a and free-space wave number k_0 are in a range where neither the electrostatic approximation[1] nor the WKB approximation[2] adequately describes the scattering problem. The full set of Maxwell's equations has to be solved which requires, in general, numerical integration.[3] For simplified boundary conditions the scattering coefficients have been determined in this way and compared with scattering measurements.[4] Both theory and experiment indicate that the *scattering* coefficient is not a very sensitive indicator for the presence of upper-hybrid resonances. Although related to the scattering problem, we will show in this paper that the *absorption* (or emission) coefficient gives a much clearer picture of the upper-hybrid resonance effects and that it is a useful parameter for plasma diagnostic applications.

The experiment is performed with quiescent afterglow plasmas produced by electrodeless rf discharge in rare gases (Ar, Ne) at low pressures (10–100 mTorr). The cylindrical column is axial to a uniform static magnetic field. The waveguide geometry is shown in Fig. 1. Absorption and emission are measured with a time-gated radiometer, described with further details of the measurement technique elsewhere.[5]

The results of the absorption measurements are given in Sec. II. The peak electron density is easily evaluated from the absorption data. The density decay is compared with ambipolar diffusion theory.

The radial density profile is investigated by a new technique described in Sec. III. A small parallel wire resonator is inserted coaxially into the plasma column and its resonant frequency is measured Similar to the cavity resonance frequency shift method, the *local* electron density is calculated from the cold-plasma perpendicular dielectric constant.

Section IV outlines the theoretical model for calculating the absorption coefficient after Ault.[3] Measured and computed absorption curves agree within the limits of the model.

The high absorption coefficient in the range of upper-hybrid frequencies implies by Kirchhoff's law that the noise emission approaches the blackbody limit. Assuming a Maxwellian electron-velocity distribution in collisional afterglow plasmas, emission and absorption measurements yield the electron temperature, as shown in Sec. V. Time-resolved noise measurements give the temperature decay. The *local* electron temperature is found from the fact that in a nonuniform plasma column resonant absorption and emission occur in a narrow layer satisfying the upper hybrid resonance condition $\omega_p^2(r)=\omega^2-\omega_c^2$. The radial position r of the resonant layer can be easily varied with frequency or magnetic field. These spatially and time resolved temperature measurements do not perturb the plasma and have a high accuracy even at low temperatures owing to nearly blackbody emissivity.

The existence of the upper-hybrid resonance layer is experimentally verified in a heating experiment described in Sec. VI. An incident microwave heating pulse is shown to raise the electron temperature in a

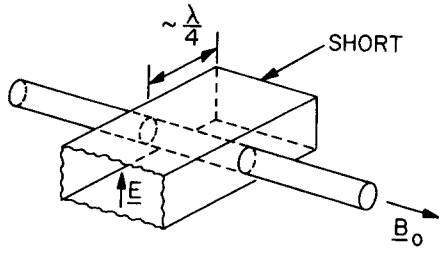

FIG. 1. Arrangement of the plasma column and the TE_{10}-mode waveguide. A perfect short produces a standing-wave maximum in the column center in the absence of plasma.

Downloaded 10 Feb 2006 to 131.215.225.175. Redistribution subject to AIP license or copyright, see http://jap.aip.org/jap/copyright.jsp

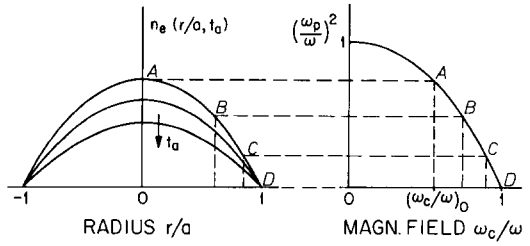

FIG. 2. The decaying radial density profile $n_e(r, t_a)$ and the upper-hybrid resonance relation $(\omega_p/\omega)^2 = 1 - (\omega_c/\omega)^2$ determine the range in magnetic fields for which the nonuniform plasma column sustains resonances, $(\omega_c/\omega)_0 \leq \omega_c/\omega \leq 1$ (A to D).

layer whose local upper-hybrid frequency corresponds to the heating frequency.

Section VII summarizes the results of the emission and absorption measurements.

II. ABSORPTION MEASUREMENTS

The absorption coefficient A of the plasma column in the waveguide arrangement of Fig. 1 is determined by measuring the reflected power P_r for a constant incident power P_i. The waveguide short is placed a quarter guide wavelength behind the plasma column so as to produce an open circuit at the plasma itself. Since there is no transmitted signal in the shorted guide we simply have

$$A = 1 - P_r/P_i. \tag{1}$$

Calibration points are obtained with a perfect short ($P_r = P_i$) and a matched termination ($P_r = 0$). Radiation through the holes in the waveguide sidewalls and losses in the quartz tube are negligible compared with the resonant plasma absorption.

Absorption measurements are most conveniently done at a fixed signal frequency ω while varying the magnetic field. Resonant absorption occurs only when the signal frequency equals the upper-hybrid frequency ω_{uh}, i.e., when

$$\omega^2 = \omega_{uh}^2(r) = \omega_c^2 + \omega_p^2(r), \quad 0 \leq r \leq a \tag{2}$$

where ω_c is the electron cyclotron frequency, $\omega_p(r)$ the local plasma frequency, and a the column radius.

The electron density in the decaying plasma is a decreasing function with radial position r and afterglow time t_a (see Fig. 2). When, at a given afterglow time the magnetic field is increased from zero, the resonance condition is first satisfied at the maximum electron density A. The corresponding normalized magnetic field $(\omega_c/\omega)_0 = [1 - \omega_{p\,max}^2/\omega^2]^{1/2}$ will be denoted as the *onset* magnetic field. A continuous range of upper-hybrid resonances exists for magnetic fields between $(\omega_c/\omega)_0$ and $\omega_c/\omega = 1$ (A to D). With increasing magnetic field, the location of the resonance shifts toward lower densities, i.e., toward the wall D. Upper-hybrid resonance does not occur beyond $\omega_c/\omega = 1$.

Figure 3 shows a typical behavior of the measured power-absorption coefficient vs normalized magnetic field at different times in the afterglow. The range of resonant absorption is clearly defined. It narrows as the peak density decreases later in the afterglow. The *maximum* absorption coefficient reaches $A \simeq 1$ and does not change over large parts of the afterglow. The exact shape of the absorption curve depends on various factors such as the density profile, the properties of the quartz tube, the column dimensions compared to the waveguide size, and fringing fields of the waveguide holes. The latter are probably responsible for exciting whistler modes at higher densities, causing the narrow absorption line at $\omega_c/\omega \gtrsim 1$.

Besides the high value of the absorption coefficient, the most useful quantity is the well-defined onset from which the peak electron density is easily derived.[6] If the waveguide were terminated in a matched load the reflected or transmitted signal would not show such a clearly defined onset since the reactive scattering is not simply confined to the upper-hybrid resonance range. For this reason earlier scattering experiments were not as easy to interpret.[7]

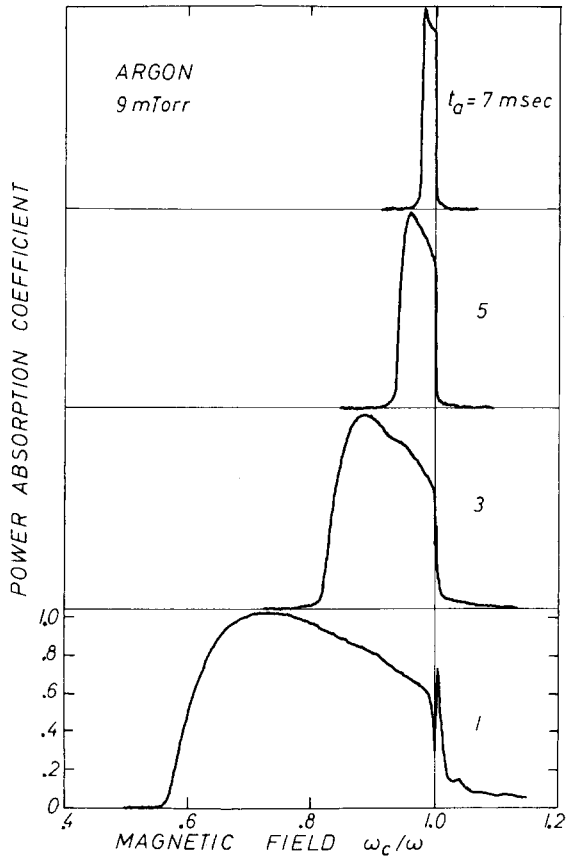

FIG. 3. Power absorption coefficient vs normalized magnetic field for different afterglow times t_a of an argon plasma column in an S-band waveguide (column diam 20 mm, waveguide RG 48U, frequency $\omega/2\pi = 3000$ MHz, test signal power -70 dBm). The lower absorption scale applies to all curves.

Downloaded 10 Feb 2006 to 131.215.225.175. Redistribution subject to AIP license or copyright, see http://jap.aip.org/jap/copyright.jsp

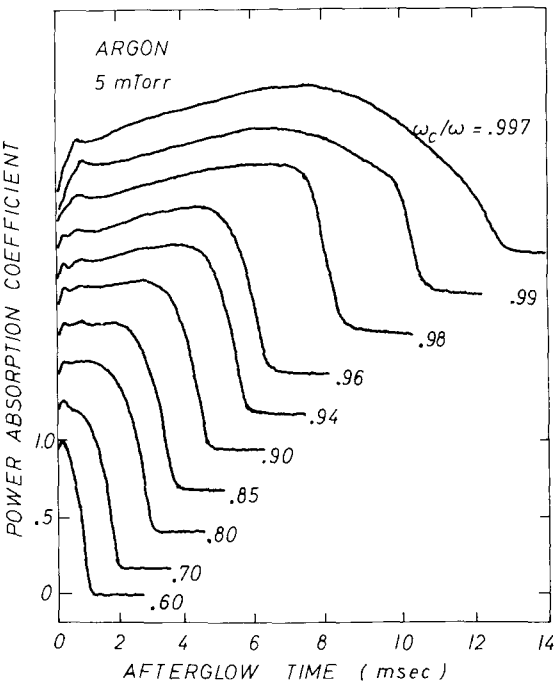

FIG. 4. Absorption coefficient vs afterglow time with normalized magnetic field as parameter. The curves are displaced for purpose of display; the lower absorption scale applies to each curve. Note the well-defined end points of absorption where the signal frequency equals the peak upper-hybrid frequency.

For the purpose of peak-density evaluation an even simpler measurement gives the same result. Figure 4 shows the absorption coefficient vs afterglow time for different magnetic fields as can be directly observed on an oscilloscope. Resonant absorption vanishes quite abruptly at an afterglow time when the peak electron density yields a maximum upper-hybrid frequency equal to the signal frequency. Figure 4 may also be thought of as a vertical cut through Fig. 3.

A typical decay curve for the peak electron density is shown in Fig. 5. In the present regime the plasma decays by ambipolar diffusion. However, at low neutral pressures, low electron temperatures, and high electron densities, the electron-neutral collision frequency is negligible compared with the electron-ion collision frequency. The plasma then behaves more like a fully ionized gas. The diffusion equation becomes nonlinear and no analytic solution exists for the density profile and decay time.[8]

As an approximation we estimate the decay time by considering parallel and perpendicular decay independently and set

$$1/\tau_{\text{tot}} \simeq 1/\tau_{\parallel} + 1/\tau_{\perp}. \tag{3}$$

The parallel ambipolar decay time is given by[8]

$$\frac{1}{\tau_{\parallel}} = \left(\frac{\pi}{L}\right)^2 \frac{k(T_e + T_i)}{m_i \nu_{in}}, \tag{4}$$

where L is the column length, kT_e and kT_i the electron and ion energies, m_i the ion mass, and ν_{in} the ion-neutral collision frequency. The perpendicular decay time has been found by successive approximations[8]

$$\frac{1}{\tau_{\perp}} = \frac{2.15}{a^2}\left(\frac{\nu_{ei}}{\omega_c}\right)^2 \frac{k(T_e + T_i)}{m_e \nu_{ei}}, \tag{5}$$

where ν_{ei} is the peak electron-ion collision frequency and m_e is the electron mass. Using the measured electron temperature the calculated and observed decay times τ at three different afterglow times are compared in Table I. General agreement for the magnitude of the decay time is obtained, but the calculated variation with afterglow time is not as good.

So far the influence of the magnetic field variation on the density decay time has been neglected. However, with decreasing magnetic field the density in the afterglow is reduced due to enhanced perpendicular diffusion. Assuming equal initial conditions, the density change $\Delta n/n$ at afterglow time t_a due to a small magnetic field change $\Delta\omega_c/\omega_c$ is given by

$$\Delta n/n = -2(t_a/\tau_{\perp})(\Delta\omega_c/\omega_c). \tag{6}$$

When the decay is governed by perpendicular diffusion it is preferable to choose the signal frequency instead of the magnetic field as a parameter in Fig. 4. The frequency dependence of the waveguide system may alter the shape of the absorption curves but does not influence the location of the absorption onset.

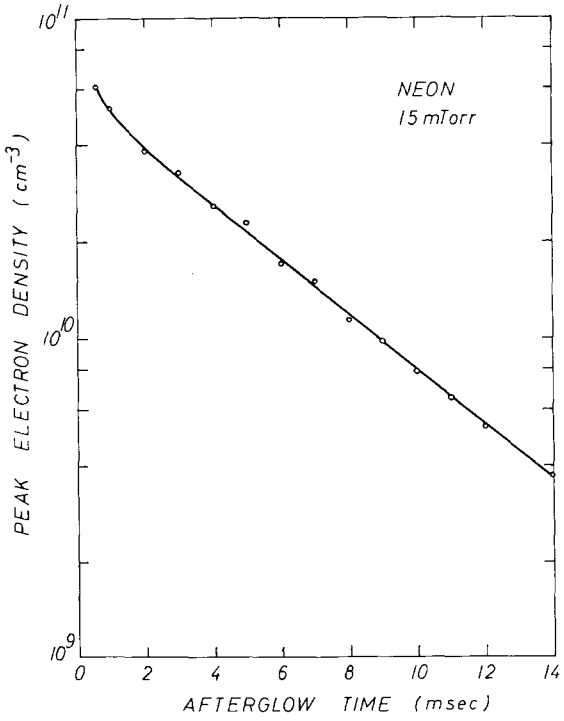

FIG. 5. Peak electron density decay in a neon plasma column at 15 mTorr (column diam 20 mm, length 40 cm, $B_0 \simeq 1$ kG).

Downloaded 10 Feb 2006 to 131.215.225.175. Redistribution subject to AIP license or copyright, see http://jap.aip.org/jap/copyright.jsp

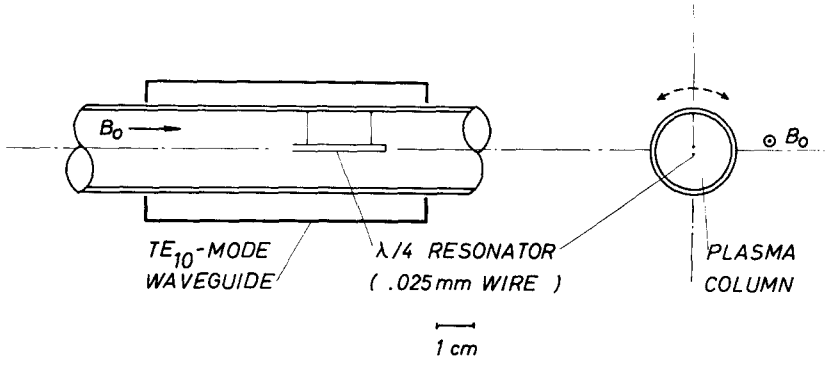

FIG. 6. The radial electron density profile is derived from the resonance frequency shift of a $\frac{1}{4}\lambda$ parallel-wire resonator suspended in the plasma column ($f_{res} \propto \epsilon_1^{-1/2}$). It is excited by the TE_{10}-mode waveguide field and can be swept radially by rotating the plasma column.

III. DENSITY PROFILE MEASUREMENTS

In order to determine the radial density profile, spatially resolved density measurements are made within the plasma. Investigations of the density perturbation of various probes and antennas in an upper-hybrid discharge (see Sec. VI) have led to the design of a quarter-wavelength parallel-wire resonator as shown in Fig. 6. Except for the fringing fields at the open end the electric field is always perpendicular to the static magnetic field so that the resonant frequency ω is given by

$$\omega = \omega_0[1 - \omega_p^2/(\omega^2 - \omega_c^2)]^{-1/2}, \tag{7}$$

where ω_0 is the vacuum resonant frequency and ω_p is the *average* local plasma frequency at the resonator. The resonator couples to the TE_{10}-mode waveguide fields so that no perturbing coaxial feeder passes through the plasma. In order to minimize the density perturbations the resonator is made of 0.001-in. silver wire (1.5 mm spacing, 2.5 cm length) and suspended on 0.0003-in. glass-wool filaments from the top of the column. The radial position is varied by rotating the quartz tube, thereby eliminating the need for a movable vacuum feedthrough. The absorption line ($A \simeq 0.4$) is observed vs afterglow time (i.e., ω_p^2) with frequency or magnetic field as parameter. For $\omega < \omega_0$ the resonance lies in the range $\omega_c/\omega > 1$; for $\omega > \omega_0$ it occurs at $\omega_c/\omega < 1$ for densities lower than those giving rise to upper-hybrid resonances.

This method gives only the radial *variation* of the plasma frequency $\omega_p^2(r)/\omega_p^2(0)$ rather than absolute values because of the presence of sheaths, fringing fields at the open end, shadows from the shorted end, etc., which are neglected here. Presumably these affect only the absolute calibration of the method. The absolute peak density is determined from the the absorption onset. The presence of the resonator in the column center reduces the peak density by less than 5%. The spatial resolution is roughly given by the wire spacing as indicated by the distance to the side walls where the frequency is shifted by the quartz dielectric.

Typical density profile measurements are shown in Fig. 7. With increasing afterglow time some steepening of the profile is observed. The measured profiles lie between the limiting cases of diffusional profiles for Coulomb collisions ($n^{(1)}$) and for constant electron-neutral collisions ($n^{(2)}$) [8]:

$$n^{(1)} \simeq n_0[1 - \tfrac{4}{3}(r/a)^2 + \tfrac{1}{3}(r/a)^4]^{1/2}, \tag{8}$$

$$n^{(2)} = n_0 J_{0[2.405(r/a)]}. \tag{9}$$

A parabolic profile may be considered as a reasonable approximation.

IV. THOERY OF THE ABSORPTION COEFFICIENT

A theoretical investigation of the absorption coefficient has been made for a model close to the experimental situation.[3] The scattering of a cold nonuniform plasma column in a parallel-plate waveguide is calculated numerically. Neglecting all variations in the axial direction and assuming an incident TEM wave, Maxwell's equations and the hydrodynamic equations can be combined to a set of first-order linear differential equations. After expanding the azimuthal dependence in the form $\Sigma_m f_m(r)e^{-im\theta}$ the fields inside the plasma in the mth mode are given by

$$\frac{d}{d\rho}(\rho E_\theta) + imE_r = -i\rho B, \tag{10}$$

$$mB = -\rho(K_1 E_r + iK_2 E_\theta), \tag{11}$$

TABLE I. Comparison between measured and calculated decay times for a neon plasma column at 15 mTorr neutral gas pressure. Electron-neutral collision frequency (Ref. 9) $\nu_{en} \simeq 10^6$ sec^{-1}; ion-neutral collision frequency (Ref. 9) $\nu_{in} = 2.1 \times 10^5$ sec^{-1}; ion temperature (assumed) $T_i = 300$ °K; cylinder dimensions $L = 40$ cm, $a = 1$ cm.

t_a	msec	1	5	10
n_{eo}	10^{10} cm^{-3}	5.2	1.3	0.8
T_e	°K	700	365	300
$\langle \nu_{el} \rangle$	10^8 sec^{-1}	0.85	0.99	0.47
$\tau_{\parallel}$	msec	8.2	13.5	13.5
$\tau_{\perp}$	msec	6.7	8.8	18.5
τ_{calc}	msec	3.7	5.3	7.8
τ_{meas}	msec	3	5	5

Downloaded 10 Feb 2006 to 131.215.225.175. Redistribution subject to AIP license or copyright, see http://jap.aip.org/jap/copyright.jsp

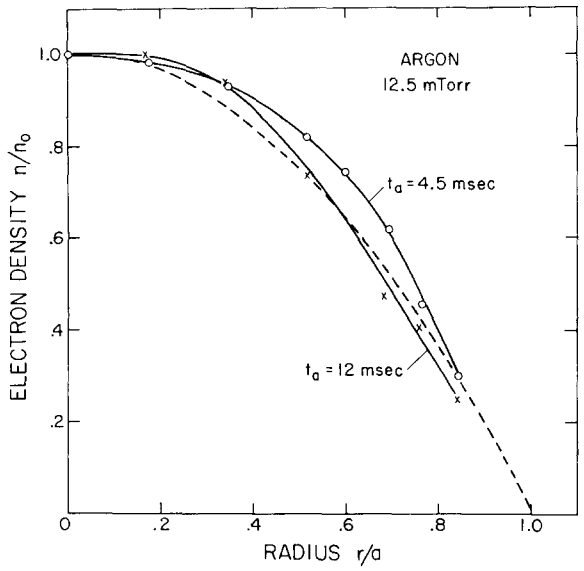

FIG. 7. Radial electron density profiles at different afterglow times in a magnetized plasma column (20 mm i.d.). The dashed line represents a parabolic profile.

$$\frac{d}{d\rho}(B) = -(K_2 E_r + iK_1 E_\theta), \tag{12}$$

where

$$\rho = (\omega/c)r = k_0 r, \quad B = cB_z,$$

$$K_1 = K_1(r) = 1 + \frac{\omega_p^2(r)/\omega^2(1 - i\nu/\omega)}{\omega_c^2/\omega^2 - (1 - i\nu/\omega)^2},$$

$$K_2 = K_2(r) = \frac{[\omega_p^2(r)/\omega^2](\omega_c/\omega)}{\omega_c^2/\omega^2 - (1 - i\nu/\omega)^2}.$$

The boundary conditions imply a regular solution at the origin $r = 0$ and an outward traveling scattered wave for $r \to \infty$. Without a waveguide structure the total field outside of the plasma column is given by the linear superposition of the incident and scattered fields

$$cB_z^{\text{ext}} = \sum_{m=-\infty}^{\infty} [i^{-m} J_{m(\rho)} + S_m H_{m(\rho)}^{(2)}] e^{-im\theta}, \tag{13}$$

$$E_r^{\text{ext}} = \frac{i}{\rho}\frac{\partial}{\partial\theta}(cB_z^{\text{ext}}), \tag{14}$$

$$E_\theta^{\text{ext}} = i\frac{\partial}{\partial\rho}(cB_z^{\text{ext}}), \tag{15}$$

where S_m is the scattering coefficient of the mth angular mode.

Plasma and free space are separated by the glass tube. In this region the appropriate solution of the wave equation is a linear superposition of Bessel and Neumann functions.

Matching the tangential field components at the outer and inner glass boundary yields the expansion coefficients, in particular the scattering coefficients S_m. Scattering and absorption cross sections are then given by

$$\sigma_s = \frac{4}{k_0}\sum_{m=-\infty}^{\infty} |S_m|^2, \tag{16}$$

$$\sigma_a = -\frac{4}{k_0}\sum_{m=-\infty}^{\infty} [|S_m|^2 + \text{Im}(S_m i^{m+1})]. \tag{17}$$

The presence of the parallel-plate waveguide complicates the solution due to mixed boundary conditions. Within the waveguide region the fields can be found by replacing the conducting walls by an infinite set of real and image columns in free space.[3] The total free-space field is then the sum of the incident plane wave and the scattered field from an array of columns.

The scattering coefficients have been solved numerically from a set of simultaneous linear equations by Ault.[3] Reflection and absorption coefficients are then found from expressions similar to Eqs. (16) and (17).

A calculated curve of the absorption coefficient vs normalized magnetic field is shown in Fig. 8. The indicated experimental parameters correspond to typical experimental conditions. The calculation shows that the main contribution of the scattering comes from the azimuthal mode $m = 1$, i.e., from those field components which rotate in the same sense as the electrons in the static magnetic field.

Low collision frequencies yield absorption curves sharply confined to the range of upper-hybrid resonances. In the limit of zero collision frequency ($\nu/\omega \to 0$) the resonant wave absorption does not vanish which is a well-known result of the singular layer concept.[7] The presence of the glass tube influences shape and magnitude of the absorption coefficient. As the theoretical model considers a simpler waveguide structure than that of the actual experiment, the comparison between calculated and measured absorption curves remains semiquantitative. However, it is a closer comparison than in previous investigations[4] where scattering coefficients calculated for a column in free space are compared with coefficients measured in a waveguide geometry.

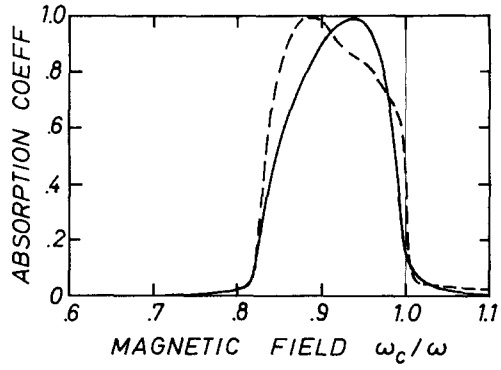

FIG. 8. Calculated absorption coefficient of a plasma column in a parallel-plate waveguide (solid curve, after Ault, Ref. 3) compared with measured absorption in a rectangular waveguide (dashed curve) (argon, 9 mTorr; $t_a = 3$ msec; quartz tube, 20 mm i.d., 23 mm o.d.; $\omega_{p\,\max}^2/\omega^2 = 0.33$; $\nu/\omega = 0.0016$, parabolic density profile).

Downloaded 10 Feb 2006 to 131.215.225.175. Redistribution subject to AIP license or copyright, see http://jap.aip.org/jap/copyright.jsp

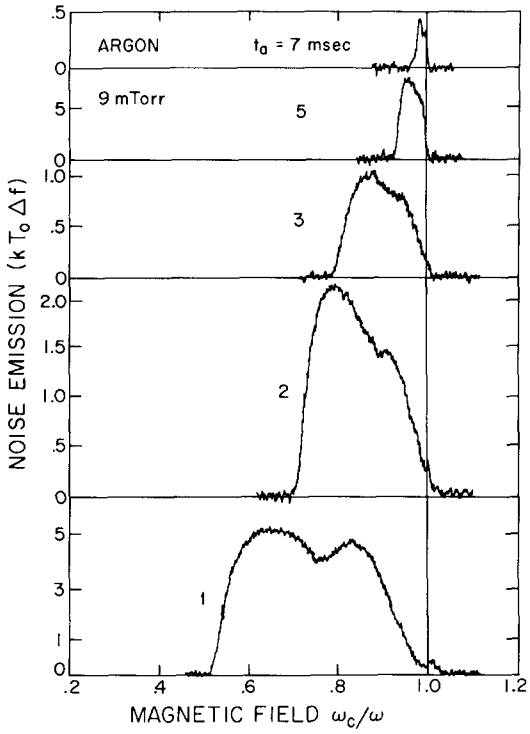

FIG. 9. Noise emission $Ak(T_{pl} - T_0)\Delta f$ vs normalized magnetic field at different afterglow times t_a of an argon plasma column (20 mm i.d.). The noise power is expressed in units of room-temperature blackbody noise $kT_0\Delta f$. Emission is confined to the range of upper-hybrid resonances.

V. EMISSION MEASUREMENTS

In the single-mode waveguide the noise power P_N emitted by the plasma column in a frequency band Δf can be expressed by[10]

$$P_N = AkT_{\text{rad}}\Delta f, \tag{18}$$

where A is the absorption coefficient, k the Boltzmann constant, and T_{rad} the electron radiation temperature. In general the radiation temperature depends on the mechanism of radiation, the distribution function, frequency and direction of observation, collective effects, etc.; but when the electrons have an equilibrium velocity distribution the radiation temperature reduces to the true electron temperature

$$T_{\text{rad}} = T_e = (3k)^{-1} m_e \bar{v}_e^2, \tag{19}$$

where $\bar{v}_e^2$ is the mean-square thermal electron velocity.

The absence of strong electric fields in afterglow plasmas and the high number of interparticle collisions leads to a Maxwellian velocity distribution. The relaxation time is given by Spitzer[11]:

$$t_{ce} = 0.266(T_e^{3/2}/n_e \ln\Lambda) \text{ in sec}, \tag{20}$$

where n_e is the electron density in cm^{-3}, $\ln\Lambda$ the Coulomb logarithm, and T_e is in °K. Observations of the "Maxwellization" in the early afterglow are in general agreement with this expression.[12] For the present conditions at the end of an rf breakdown pulse ($n_e \simeq 10^{11}$ cm^{-3}, $T_e \simeq 10\,000$ °K) we find $t_{ce} \simeq 0.25$ μsec. Since the temperature measurements are made at much later afterglow times, we consider Eq. (19) to hold.

The typical behavior of the emitted noise power vs magnetic field at different afterglow times is shown in Fig. 9. Comparison with Fig. 3 shows the very similar behavior of emission and absorption as expected from Eq. (18). Significant emission is only found in the range of high absorption, i.e., in the range of upper-hybrid resonances. Since the emission onset agrees with the absorption onset, emission measurements can also be used to determine the peak electron density. However, the decreasing signal-to-noise ratio in the late afterglow reduces the measurement accuracy. The emission maximum does not stay constant for different afterglow times, as observed for the absorption maximum, but decreases in proportion to the electron temperature. Likewise, the different shape of emission and absorption curves results from the variation of the electron temperature with magnetic field.

While it is possible to determine the electron temperature from separate emission and absorption measurements, the accuracy of the data is poor owing to the addition of both measurement errors. Therefore the electron temperature is measured directly with the aid of a blackbody reference noise source connected to the waveguide with the plasma column.[5] A time-gated radiometer measures the power flow in both directions of the waveguide. With

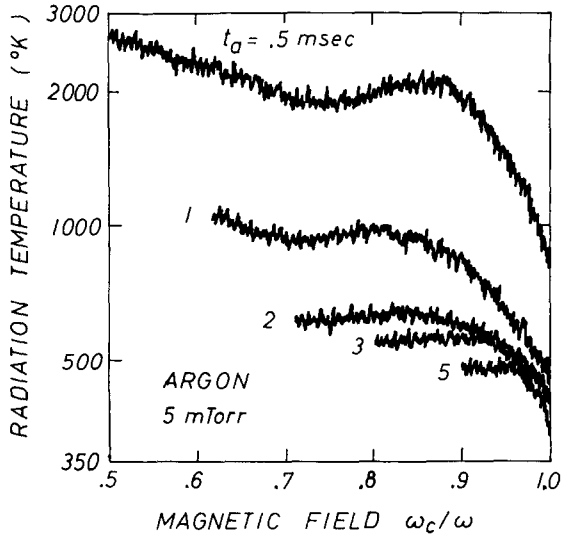

FIG. 10. Radiation temperature in argon vs normalized magnetic field at different afterglow times t_a. The temperature can only be measured in the range of upper-hybrid frequencies which narrows with increasing afterglow time. The temperature drop near $\omega_c/\omega = 1$ shows the radial decrease of the electron temperature near the side walls.

Downloaded 10 Feb 2006 to 131.215.225.175. Redistribution subject to AIP license or copyright, see http://jap.aip.org/jap/copyright.jsp

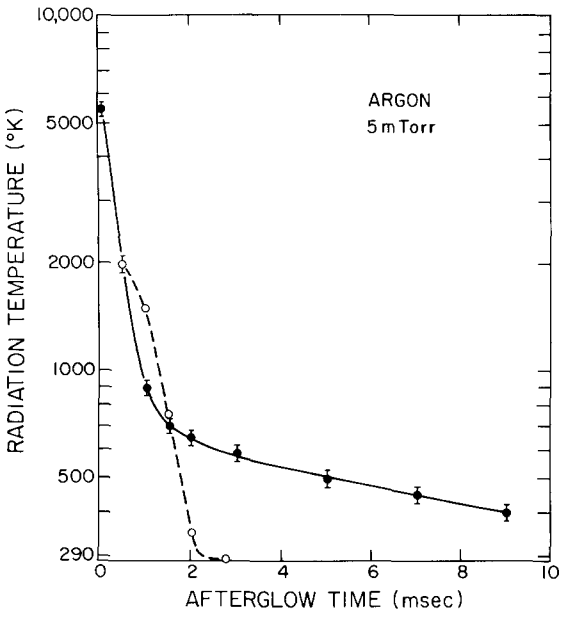

FIG. 11. Temperature decay of the electrons in the center region of the plasma column [$\omega_c/\omega \simeq (\omega_c/\omega)_0$]. The dashed curve is the calculated temperature relaxation due to electron elastic collisions with the ions at room temperature. The vertical bars indicate the temperature fluctuations due to finite integration time of the radiometer (RC = 0.1 sec).

a precision attenuator the reference temperature is adjusted for equal power flow (power emitted by plasma balances power absorbed from reference) so that the unknown radiation temperature equal to the electron temperature in equilibrium is simply given by the known reference temperature. A servoloop maintains noise power balance allowing us to record directly the electron temperature vs various parameters (ω_c, ω, t_a). Temperature measurements can only be made in the range of frequencies where upper-hybrid resonances occur, since both absorption and emission essentially vanish elsewhere. For given noise-power fluctuations (determined by the radiometer noise figure, bandwidth, integration time, and sampling duty ratio) the uncertainty in the temperature measurement increases with decreasing absorption coefficient ($\Delta T \propto A^{-1}$). The merit of the upper-hybrid resonance effect lies in obtaining a high absorptivity in a simple waveguide geometry with a minimum of plasma volume.

The radiation temperature vs magnetic field at different times in the afterglow is shown in Fig. 10. Both theory[3] and observation (Sec. VI) show that resonant absorption and emission are confined to a layer in the plasma column which satisfies the upper-hybrid resonance condition. The measured temperature then refers to the electrons in this layer, so we obtain spatial as well as temporal resolution. As the density gradient is perpendicular to the magnetic field, the electrons are strongly confined to the layer and different temperatures may be observed in different layers. For a parabolic radial density profile the location of the emitting and absorbing resonant layer as a function of normalized magnetic field is given by

$$\frac{r}{a} = \left(\frac{(\omega_c/\omega)^2 - (\omega_c/\omega)_0^2}{1 - (\omega_c/\omega)_0^2} \right)^{1/2}, \tag{21}$$

where a is the column radius. The temperature data near $(\omega_c/\omega)_0$ refer to the column center and near $\omega_c/\omega = 1$ to the wall. Note that on a linear magnetic field scale the region near the wall is expanded.

The measurements show that the radiation temperature has only small variations over most of the cross section but that it drops significantly near the wall. The latter is thought to be caused by escape of fast electrons. Since electron cooling by elastic Coulomb collisions is strongest in the region of highest density, a slight temperature minimum may be expected in the column center. The observed temperature rise with decreasing magnetic field beyond the minimum is possibly a background effect due to the large magnetic field variation similar to that in a positive column.[13]

The decay of the electron temperature in the center region of the column is shown in Fig. 11. The fast temperature decay in the early afterglow is followed by a slow decay in the low-temperature range. Considering the energy transfer in elastic collisions as the main cooling mechanism, the temperature decay is described by the equation

$$\frac{dT_e}{dt} = -\frac{1}{\tau_e}(T_e - T_0), \tag{22}$$

where the energy relaxation time τ_e is given by

$$\tau_e = (2m_e/m_i\nu_{ei})^{-1}. \tag{23}$$

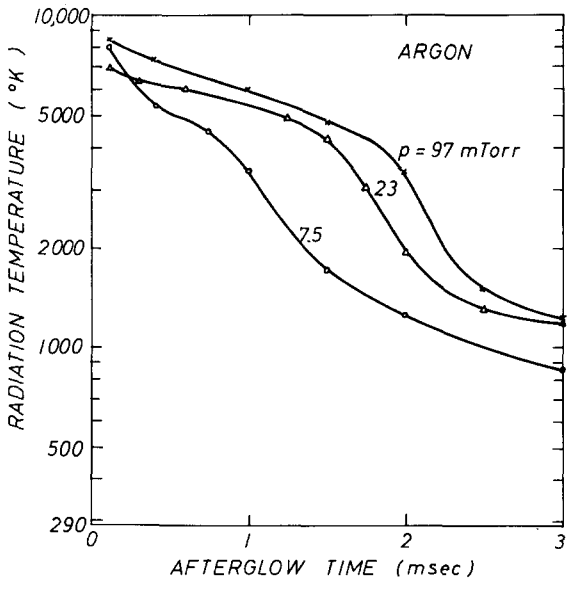

FIG. 12. Decay of the electron radiation temperature in argon at different neutral gas pressures p. In the later afterglow the electron temperature does not decrease with increasing pressure excluding the possibility that electrons have thermalized with ions at an elevated temperature.

Downloaded 10 Feb 2006 to 131.215.225.175. Redistribution subject to AIP license or copyright, see http://jap.aip.org/jap/copyright.jsp

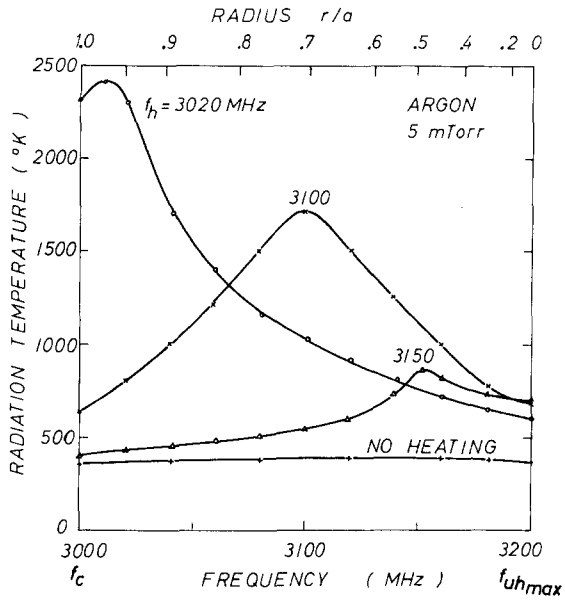

FIG. 13. Electron radiation temperature vs receiver frequency in an argon afterglow plasma heated by a microwave pulse with frequency f_h in the spectrum of upper-hybrid frequencies (3000—3200 MHz). The temperature is measured 30 μsec after the end of a 500-μsec 10-μW heating pulse applied at 7 msec in the afterglow. For a parabolic radial density profile the location of the hybrid layer is shown on the top scale.

Here ν_{ei} is the electron-ion collision frequency for momentum transfer ($\nu_{ei} \propto n_e T_e^{-3/2}$, $\nu_{ei} \gg \nu_{en}$), m_e/m_i the electron-ion mass ratio, and the ions are assumed to be at temperature T_0. For the observed exponential density decay Eq. (22) can be solved analytically. The solution is matched to the experimental conditions at $t_a = 0.5$ msec and shown as the dashed curve in Fig. 11. The predicted decay has about the same time constant as observed in the early afterglow but fails to describe the slow late afterglow decay.

The possibility of an elevated ion temperature in the late afterglow must be excluded, since the ions thermalize to the neutral gas temperature with time constant $\tau_i \simeq 10$ μsec. An experimental evidence for cold ions is shown in Fig. 12. If in the later afterglow the electrons had thermalized with hot ions, an increase in the neutral gas pressure would lower $T_e = T_i$ which we do not observe. The pressure dependence also verifies that electron-neutral collisions are unimportant under present conditions.

The unexpectedly high electron temperatures in afterglows as observed in many other experiments[14] have been explained by collisions of electrons with metastable ions. The electrons gain energy by deexciting the metastable ions.[15] Even a very small number of energy-transfering collisions is sufficient to raise the electron temperature, since electrons in argon have to undergo about $m_i/2m_e \simeq 40\,000$ elastic collisions to lose most of the energy gained in one deexciting collision. Using only a standard high-vacuum station (base pressure 3×10^{-7} Torr, not bakeable) the presence of long-lived nitrogen metastables as impurities is very likely. A detailed study of atomic processes was not the main objective of this investigation, although the combined temperature and density measurement provides an excellent basis for it.

VI. UPPER-HYBRID RESONANCE HEATING

The main purpose of the heating experiment is to show the existence of the resonant absorption layer. The results of upper-hybrid resonance heating will, however, be of interest in other respects as well.

If the previous interpretation of localized wave absorption is correct, it should be possible to heat the electrons in the resonant layer by an intense microwave pulse and, after "Maxwellization," observe a maximum in the radial temperature profile. The present arrangement is very well suited for this experiment, since the magnetic field is perpendicular to the density gradient, thereby inhibiting rapid heat exchange between different radial layers. Thus the heated layer is expected to be seen for appreciable times, roughly on the order of the energy relaxation time. These observations will fully utilize the unique feature of sensitive nonperturbing temperature measurements with spatial and temporal resolution.

The experiment is performed in the late afterglow where the electron temperature without heating is uniform and close to room temperature. The magnetic field is held constant in order to heat only a single layer for a given heating pulse frequency. The temperature profile is measured by sweeping the

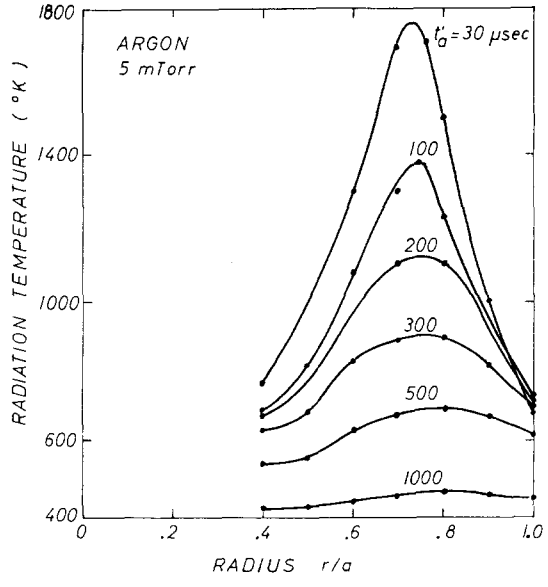

FIG. 14. Radiation temperature profiles of a heated afterglow plasma at different times t'_a after the end of the heating pulse. The radial scale is based on a parabolic density profile. Other experimental parameters are the same as in Fig. 13 ($f_h = 3100$ MHz).

Downloaded 10 Feb 2006 to 131.215.225.175. Redistribution subject to AIP license or copyright, see http://jap.aip.org/jap/copyright.jsp

radiometer frequency through the range of upper-hybrid frequencies which becomes narrow in the later afterglow so that the frequency response of the system is sufficiently flat. The latter is only of importance with respect to the temperature fluctuations but does not change the desired average value. Figure 13 shows the radial temperature profile without and with heating for three different heating pulse frequencies f_h. The heating pulse of duration $t_h = 500$ μsec and power $P_h = 10$ μW is applied at $t_a = 7$ msec in the afterglow. The electron temperature is measured at $t_a' = 30$ μsec after the end of the heating pulse.

When the frequency of the heating pulse lies in the range of upper-hybrid frequencies we observe a strong temperature rise showing a maximum when the observation frequency equals the heating frequency. At the present power level the heating pulse leaves the electron density unchanged as concluded from separate absorption measurements. Thus the observed temperature maximum leads to the conclusion of preferred wave absorption in a layer whose local upper-hybrid frequency equals the heating frequency. The three different heating frequencies show the consistency of the result (see Fig. 13).

As the measured temperature profile represents the convolution of the true temperature profile with the observed layer of finite width, the true shape of the heated layer is sharper than indicated in Fig. 13. The finite radiometer bandwidth ($\Delta f \simeq 20$ MHz) results in a slight loss of spatial resolution, but is necessary to keep the output fluctuations at a low level ($\Delta T \propto B^{-1/2}$). The observed layer is also broadened by other effects such as the slow density decay during the experiment, density fluctuations among different afterglows, and the time lag between heating and temperature measurement during which the electrons cool. Qualitatively the measurements shows that the hybrid layer becomes narrower near the wall where the density gradients are steep. For a constant heating pulse energy the electron temperature assumes higher values in a thin layer involving fewer electrons. When the heating frequency lies beyond the hybrid resonance range no heating effects are observed at the same pulse energy.

The relaxation of the heated layer has been observed by varying the observation time after the end of the heating pulse. The results are shown in Fig. 14. The linear radial scale is based on a parabolic density profile which is a close approximation to the observed profiles. The strong magnetic field restricts the radial energy transport so that the temperature peak decays on the time scale of the collisional relaxation time.

As the plasma column is nearly a perfect absorber, the energy of the microwave heating pulse is thought to be converted into kinetic energy of the electrons. A simple calculation of the energy balance is in agreement with this picture. We assume that there are no axial temperature gradients but a cosinusoidal axial density profile due to ambipolar diffusion. The total energy increase of all electrons is found by integrating the energy gain per volume element $n_e \Delta k T_e$ over the entire plasma column:

$$W = \int_{-L/2}^{L/2} \int_0^a n_e(r, z) k \Delta T_e(r) 2\pi r \, dr \, dz. \tag{24}$$

The density profile is taken to be

$$n_e = n_{e0}(1 - r^2/a^2)\cos(\pi z/L), \tag{25}$$

where a and L are the cylinder radius and length. For the measured temperature profile at $t_a' = 30$ μsec in Fig. 14, the numerical integration of Eq. (24) yields

$$W = 4.6 \times 10^{-9} \text{ J}.$$

The heating pulse energy is given by

$$W = P_h t_h = 10 \ \mu\text{W} \times 500 \ \mu\text{sec} = 5 \times 10^{-9} \text{ J}.$$

Thus it appears that the incident microwave energy is efficiently converted into thermal electron energy.

The heating pulse power cannot be raised indefinitely without seriously affecting other plasma parameters. Beyond a certain threshold ($P_h \gtrsim 100$ μW, $t_h = 500$ μsec) typical indications of an instability are observed: strong microwave noise emission during the heating and density decrease due to enhanced diffusion. For heating pulse powers above $P_h \gtrsim 1$ mW ($t_h = 1$ msec) excitation and ionization occur in the resonant region. A bright annulus is visible when the plasma column is observed along its axis as shown in Fig. 15 (left-hand side). As expected, the annulus shrinks to the column center when the magnetic field is decreased and/or the heating frequency increased. The radial density profile can, however, not be derived from this effect, since it may change with different positions of the ionizing layer. The density increase is seen by raising the microwave power level which shifts the layer radially outward and increases the range in ω_h or ω_c over which it is visible.

For continous incident microwave signals with $P_h = 10$ mW the discharge is maintained continuously without previous rf (20 MHz) breakdown pulses. The discharge has to be started at cyclotron resonance and can then, with increased density, be maintained in the hybrid resonance range. This microwave breakdown behavior has previously been observed[16] but not explained by the upper-hybrid resonance.

As a simple application of the upper-hybrid resonance breakdown we investigated qualitatively the density perturbation by probes in nonuniform plasmas. In a uniform magnetic field the visible resonance layer represents a contour of constant density. Figure 15 (right-hand side) shows the deformation of the density contour due to a probe coaxial with the

Downloaded 10 Feb 2006 to 131.215.225.175. Redistribution subject to AIP license or copyright, see http://jap.aip.org/jap/copyright.jsp

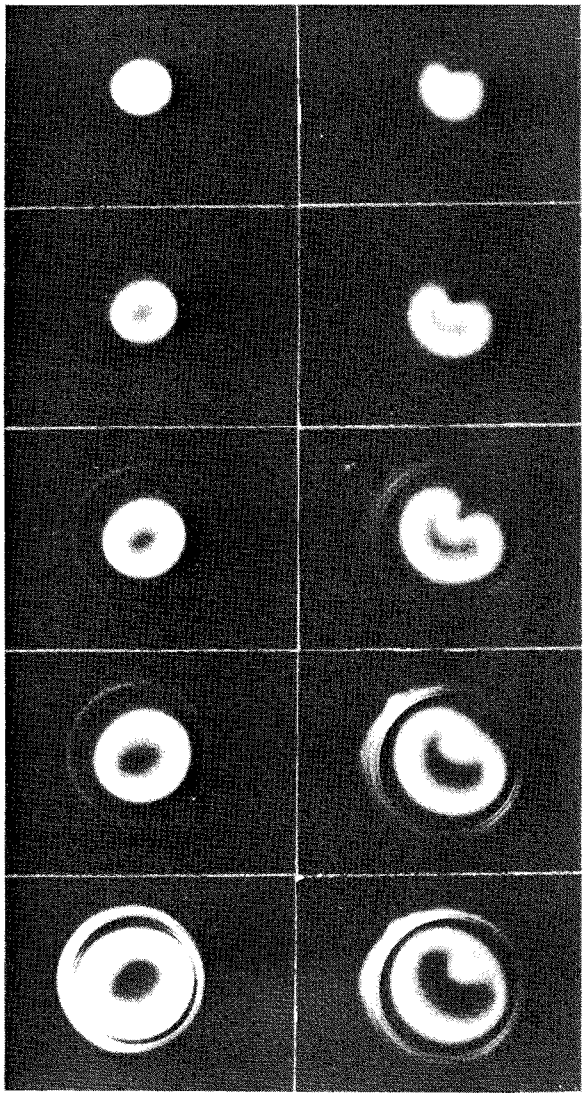

FIG. 15. *Left*: Appearance of an argon plasma column produced by microwave breakdown in the range of upper-hybrid frequencies (axial view). The outside bright ring is due to light reflections at the walls of the quartz cylinder. The resonant layer shrinks to the column center as the magnetic field is decreased and/or the signal frequency increased (argon 12 mTorr, $P_h = 100$ mW, 20 mm column i.d.). *Right*: The density profile is perturbed by the presence of an antenna parallel to the magnetic field, slightly off center (argon 5 mTorr, $P_h = 50$ mW, antenna diam 0.6 mm, length 40 mm).

column axis and slightly off center (dimensions: 40 mm length, 0.6 mm diam). The density drop near the probe is indicated by a small hybrid layer around it and by the radial inward deformation of the original annulus. Reducing the diameter to 0.025 mm essentially eliminates the perturbation.

VII. SUMMARY AND CONCLUSIONS

The experimental investigation of the upper-hybrid resonance effects in a nonuniform plasma column confirms the predicted cold-plasma resonant-wave absorption.[3] Particularly, we could show that in regions of density gradients resonant absorption and emission are spatially confined to a resonant layer.

Absorption and emission measurements in the range of upper-hybrid frequencies are a powerful method of nonperturbing afterglow plasma diagnostics. The peak electron density can be determined over one to two orders of magnitude, the electron temperature can be measured with good accuracy ($\simeq 10\%$) even at values close to room temperature. This is a result of the high absorptivity of the plasma column in the range of upper-hybrid frequencies. Compared to the cyclotron resonance, used for the same purpose in previous experiments,[13] the hybrid resonance yields spatially resolved temperature data in a nonuniform column. A resonant-probe method with least perturbations is used to obtain the density profile which, under present conditions, is approximately parabolic.

Microwave heating by upper-hybrid resonance absorption offers a method to obtain locally heated plasma regions or temperature gradients in a controlled measurable way. The plasma stability in the presence of density and temperature gradients can be investigated. Upper-hybrid resonance breakdown is an efficient method for plasma generation. It may be of importance in many magnetically confined high-density plasmas ($\omega_p \sim \omega_c$).

ACKNOWLEDGMENTS

The authors gratefully acknowledge support from the U.S. Atomic Energy Commission for this work, and various interesting discussions with R.H. Ault concerning the theoretical investigation of the absorption coefficient, and for the use of his numerical results prior to publication.

*Present address: Department of Physics, University of California, Los Angeles, California.
†Present address: U.S. Atomic Energy Commission (CTR), Washington, D.C.

[1] D. E. Baldwin, D. M. Henderson, and J. L. Hirschfield, Phys. Rev. Letters 20, 314 (1968); L. O. Bauer, F. A. Blum, and R. W. Gould, *ibid.* 20, 435 (1968).
[2] A. F. Kuckes and A. Y. Wong, Phys. Fluids 8, 1161 (1965).
[3] R. H. Ault and R. W. Gould, Bull. Am. Phys. Soc. 14, 1253 (1969); R. H. Ault (private communication).
[4] R. Greenwald and F. Boley, Phys. Fluids 13, 1380 (1970); R. Greenwald, *ibid.* 13, 1112 (1970).
[5] R. L. Stenzel and R. W. Gould, Rev. Sci. Instr. 40, 1461 (1969).
[6] This method of peak density diagnostic has earlier been used in a cylindrical cavity instead of a rectangular waveguide. S. J. Buchsbaum and A. Hasegawa, Phys. Rev. Letters 12, 685 (1964).
[7] F. A. Blum, L. O. Bauer, R. W. Gould, and R. L. Stenzel, Phys. Fluids 12, 1018 (1969).
[8] V. E. Golant and A. P. Zhilinskii, Zh. Tekh. Fiz. 32, 1313 (1962) [Sov. Phys. Tech. Phys. 7, 970 (1963)].
[9] S. C. Brown, *Basic Data of Plasma Physics* (Technology Press of M.I.T., Cambridge, Mass., 1959).
[10] G. Bekefi, *Radiation Processes in Plasmas* (Wiley, New York, 1966).

Downloaded 10 Feb 2006 to 131.215.225.175. Redistribution subject to AIP license or copyright, see http://jap.aip.org/jap/copyright.jsp

[11]L. Spitzer, Jr., *Physics of Fully Ionized Gases* (Interscience, New York, 1962).
[12]B. L. Wright, Ph. D. thesis (Massachusetts Institute of Technology, 1967) (unpublished).
[13]H. Fields, G. Bekefi, and S. C. Brown, Phys. Rev. **129**, 506 (1963).
[14]J. C. Ingraham and S. C. Brown, Phys. Rev. **138**, A1015 (1965); D. Formato and A. Gilardini, *Proceedings of the Fourth International Conference on Ionization Phenomena in Gases, Uppsala*, 1959, edited by N. Robert Nielsson (North-Holland, Amsterdam, 1960), Vol. 1, pp. 1A99–104; J. H. Noon, P. R. Blaszuk, and E. H. Holt, J. Appl. Phys. 39, 9 (1968).
[15]I. R. Hurle, J. Chem. Phys. 41, 3592 (1966).
[16]G. Lisitano, *Proceedings of the Seventh International Conference on Ionization Phenomena in Gases, Belgrade*, 1965, edited by B. Perovica and D. Tosić (Gradjerimska Knjiga, Belgrade, Yugoslavia, 1966), Vol. I, pp. 464–467.

Downloaded 10 Feb 2006 to 131.215.225.175. Redistribution subject to AIP license or copyright, see http://jap.aip.org/jap/copyright.jsp